

Multi-robot Active Target Tracking with Distance and Bearing Observations

Ke X. Zhou* and Stergios I. Roumeliotis†

*Dept. of Electrical and Computer Engineering, †Dept. of Computer Science and Engineering
University of Minnesota, Minneapolis, MN 55455 Email: {kezhou|stergios}@cs.umn.edu

Abstract—In this paper, we study the problem of *optimal trajectory generation* for a team of mobile robots tracking a moving target using distance and bearing measurements. Contrary to previous approaches, we explicitly consider limits on the robots’ speed and impose constraints on the minimum distance at which the robots are allowed to approach the target. We first address the case of a single sensor and show that although this problem is non-convex with non-convex constraints, in general, its optimal solution can be determined analytically. Moreover, we extend this approach to the case of multiple sensors and propose an iterative algorithm, *Gauss-Seidel-relaxation* (GSR), for determining the set of feasible locations that each sensor should move to in order to minimize the uncertainty about the position of the target. Extensive simulation results are presented demonstrating that the performance of the GSR algorithm, whose computational complexity is linear in the number of sensors, is indistinguishable of that of a *grid-based exhaustive search*, with cost exponential in the number of sensors, and significantly better than that of a *random, towards the target, motion strategy*.

I. INTRODUCTION

Optimally tracking a moving target under motion and processing constraints is necessary in a number of applications such as environmental monitoring, surveillance, human-robot interaction, as well as defense applications. In most cases in practice, multiple wireless *static* sensors are employed in order to improve the tracking accuracy and increase the size of the surveillance area. Contrary to static sensors, whose density and sensing range are fixed, *mobile* sensors (robots) can cover larger areas over time without the need to increase their number. Additionally, their spatial distribution can change dynamically so as to adapt to the motion of the target, and hence provide informative measurements about its position. Selecting the best sensing locations is of particular importance especially when considering time-critical applications (e.g., when tracking a hostile target), as well as limitations on the robots’ processing and communication resources.

In this paper, our objective is to determine optimal trajectories for a team of heterogeneous robots that track a moving target using *distance and bearing* measurements. Since accurately predicting the motion of the target over multiple time steps is impossible, we focus our attention to the case where the robots must determine their optimal sensing locations for one time step at a time. Specifically,

we seek to minimize the uncertainty about the position of the target, expressed as the trace of the posterior covariance matrix for the target’s position estimates, while considering maximum-speed limitations on the robots’ motion. Additionally, and in order to avoid collisions, we impose constraints on the minimum distance between any of the robots and the target (cf. Section III). Due to the non-linearities of the robots’ motion and measurement models, this formulation results in a non-convex objective function with non-convex constraints on the optimization variables (i.e., the robots’ sensing locations).

The main contributions of this work are the following:

- We first investigate the case of a *single sensor* and for the first time we prove that the optimal solution to the active target tracking problem, when using distance and bearing measurements, can be determined analytically (cf. Section IV-A). In particular, we show that depending on the distance between the robot and the target, three distinct cases must be considered, each corresponding to different pairs of polynomial equations in two variables. The solutions of these bivariate polynomial systems are computed by first employing the Sylvester resultant to eliminate one of the variables and subsequently determining the roots of the resulting univariate polynomial through the companion matrix [1].

- We extend this approach to the case of *multiple sensors* by employing the non-linear Gauss-Seidel-relaxation (GSR) algorithm whose computational complexity is linear in the number of sensors (cf. Section IV-B). Additionally, we compare the performance of the GSR algorithm to that of a grid-based exhaustive search (GBES), whose cost is exponential in the number of sensors, and show that GSR achieves comparable tracking accuracy at a significantly lower computational cost (cf. Section V).

Before describing the formulation and solution of the active target tracking problem, in Sections III and IV, respectively, we first review related work in Section II. Simulation results are presented in Section V, while the conclusions of this work and directions of future research are discussed in Section VI.

II. LITERATURE REVIEW

Although target tracking has received considerable attention, in most cases the sensors involved are *static* and the emphasis is on the optimal processing of the available

This work was supported by the University of Minnesota (DTC), and the National Science Foundation (IIS-0643680, IIS-0811946, IIS-0835637).

information (e.g., given communication constraints [2], [3]). Significant work on the problem of *single-robot* active target tracking using *bearing-only* measurements, has been presented in [4], [5], [6]. Additionally, the case of *multi-robot* active target tracking using *distance-only* measurements has been addressed in [7], [8], [9]. Due to the key differences in the observation models when distance-only or bearing-only, instead of distance *and* bearing, measurements are considered and their impact on selecting the next best sensing location, we hereafter limit our discussion to multi-robot tracking approaches that use *both distance and bearing* measurements.

Stroupe and Balch [10] propose an approximate tracking behavior, where the mobile sensors attempt to minimize the target's location uncertainty using distance and bearing measurements. The objective function is the *determinant* of the target position estimates' covariance matrix. The optimization process in this case does not consider the set of all possible trajectories. Instead, a *greedy search* is performed over the discretized set of candidate headings, separately for each sensor. Additionally, the expected information gain from the teammates' actions is approximated by assuming that the other sensors' measurements in the next time step will be the same as these recorded at their current locations.

Chung *et al.* [11] present a decentralized motion planning algorithm for solving the multi-sensor target tracking problem using both distance and bearing measurements. The authors employ the *determinant* of the target's position covariance matrix as the cost function. The decentralized control law in this case is based on the *gradient* of the cost function with respect to each of the sensor's coordinates, multiplied by constant step-size of 1. The authors, however, do not account for the speed constraints on the motion of sensors. In addition, the convergence rate of the gradient-based method and the existence of local minima are not considered.

The main drawback of the previous approaches is that no constraints on the speed of the sensors are considered. Furthermore, their impact on the computational complexity of the optimization algorithm used is not examined. The only exception is the work presented in [10]. In that case, however, these constraints are used only to define the discretized region over which the heading of each sensor is optimized *independently* (i.e., each sensor determines its next sensing location without considering the constraints on the motion of its teammates). Contrary to previous approaches, in our formulation, we account for the existence of *prior information* and explicitly consider *constraints* on the motion of the sensors (maximum speed and minimum allowed distance to the target).

III. PROBLEM FORMULATION

Consider a group of mobile sensors (or robots) moving in a plane and tracking the position of a moving target by processing distance and bearing measurements. In this paper, we study the case of *global tracking*, i.e., the position of the target is described with respect to a fixed (global) frame of

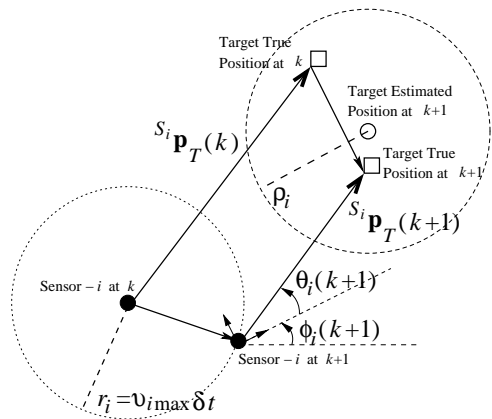


Fig. 1. Illustration of the i -th sensor's and target's motion: Sensor- i moves in 2D with speed v_i , which is bounded by $v_{i\max}$. From time-step k to $k+1$, the sensor can only move within a circular region centered at its position at time-step k with radius $r_i = v_{i\max}\delta t$. Furthermore, to avoid collision with the target, sensor- i is prohibited to move inside a circular region centered at the target's position estimate at time-step $k+1$ with radius ρ_i . $S_i \mathbf{p}_T$ is the target's position with respect to sensor- i . The distance measurement of sensor- i is the norm of $S_i \mathbf{p}_T(k+1)$ plus noise, and the bearing measurement of sensor- i is $\theta_i(k+1)$ plus noise.

reference, instead of a relative *group-centered* one. Hence, we hereafter employ the assumption that the position and orientation (pose) of each tracking sensor are known with high accuracy within the global frame of reference (e.g., from precise GPS and compass measurements).

Furthermore, we consider the case where each sensor can move in 2D with speed v_i , which is *upper bounded* by $v_{i\max}$, $i = 1, \dots, M$, where M is the number of sensors. Therefore, at time-step $k+1$, sensor- i can only move within a circular region centered at its position at time-step k with radius $r_i = v_{i\max}\delta t$ (cf. Fig. 1), where δt is the time step. In order to avoid collisions with the target, we also require that the distance between the target and sensor- i to be greater than a threshold ρ_i , i.e., sensor- i is prohibited to move inside a circular region centered at the target's position estimate at time-step $k+1$ with radius ρ_i (cf. Fig. 1). Note also that since the motion of the target can be reliably predicted for the next time step only, our objective is to determine the next best sensing locations for all sensors at consecutive time steps.

In the next two sections, we present the target's state propagation equations and the sensors' measurement model.

A. State Propagation

In this work, we employ the Extended Kalman Filter (EKF) for recursively estimating the target's state, $\mathbf{x}_T(k)$. This is defined as a vector of dimension $2N$, where $N-1$ is the highest-order time derivative of the position, $(x_T(k), y_T(k))$, described by the motion model, and can include components such as position, velocity, and acceleration:

$$\mathbf{x}_T(k) = [x_T(k) \ y_T(k) \ \dot{x}_T(k) \ \dot{y}_T(k) \ \ddot{x}_T(k) \ \ddot{y}_T(k) \ \dots]^T \quad (1)$$

We consider the case where the target moves randomly and assume that we know the stochastic model describing the motion of the target (e.g., constant-acceleration or constant-velocity, etc. [12]). However, as it will become evident later

on, our sensing strategy does not depend on the particular selection of the target's motion model.

The discrete-time state propagation equation is:

$$\mathbf{x}_T(k+1) = \Phi_k \mathbf{x}_T(k) + G_k \mathbf{w}_d(k) \quad (2)$$

where \mathbf{w}_d is a zero-mean white Gaussian noise process with covariance $Q_d = E[\mathbf{w}_d(k)\mathbf{w}_d^T(k)]$.

The estimate of the target's state is propagated as:¹

$$\hat{\mathbf{x}}_T(k+1|k) = \Phi_k \hat{\mathbf{x}}_T(k|k) \quad (3)$$

where $\hat{\mathbf{x}}_T(\ell|j)$ is the state estimate at time-step ℓ , after measurements up to time-step j have been processed.

The error-state covariance matrix is propagated as:

$$P_{k+1|k} = \Phi_k P_{k|k} \Phi_k^T + G_k Q_d G_k^T$$

where $P_{\ell|j}$ is the covariance of the error, $\tilde{\mathbf{x}}_T(\ell|j)$, in the state estimate. The state transition matrix, Φ_k , and the process noise Jacobian, G_k , that appear in the preceding expressions depend on the motion model used [12]. In our work, these can be arbitrary, but known, matrices, since no assumptions on their properties are imposed.

B. Measurement Model

At time-step $k+1$, sensor- i measures its distance $d_i(k+1)$ and bearing $\theta_i(k+1)$ to the target ($i = 1, \dots, M$), as shown in Fig. 1. Assume the orientation of sensor- i is $\phi_i(k+1)$, therefore the measurement equation is:

$$\mathbf{z}(k+1) = \begin{bmatrix} d_1(k+1) \\ \theta_1(k+1) \\ \vdots \\ d_M(k+1) \\ \theta_M(k+1) \end{bmatrix} + \begin{bmatrix} n_{d_1}(k+1) \\ n_{\theta_1}(k+1) \\ \vdots \\ n_{d_M}(k+1) \\ n_{\theta_M}(k+1) \end{bmatrix} \quad (4)$$

with ($i = 1, \dots, M$)

$$d_i(k+1) = \sqrt{\Delta x_{T_i}^2(k+1) + \Delta y_{T_i}^2(k+1)}$$

$$\theta_i(k+1) = \arctan\left(\frac{\Delta y_{T_i}(k+1)}{\Delta x_{T_i}(k+1)}\right) - \phi_i(k+1)$$

where

$$\Delta x_{T_i}(k+1) = x_T(k+1) - x_{S_i}(k+1)$$

$$\Delta y_{T_i}(k+1) = y_T(k+1) - y_{S_i}(k+1)$$

and $\mathbf{p}_T(k+1) = [x_T(k+1) \ y_T(k+1)]^T$, $\mathbf{p}_{S_i}(k+1) = [x_{S_i}(k+1) \ y_{S_i}(k+1)]^T$ are the positions of the target and the i -th sensor, respectively, expressed in the global frame of reference. Note also that $\mathbf{n}_i(k+1) = [n_{d_i}(k+1) \ n_{\theta_i}(k+1)]^T$ is the noise in the i -th sensor's measurements, which is a zero-mean white Gaussian process with covariance $R_i = E[\mathbf{n}_i(k+1)\mathbf{n}_i^T(k+1)] = \text{diag}(\sigma_{d_i}^2, \sigma_{\theta_i}^2)$, and independent of the noise in other sensors, i.e., $E[\mathbf{n}_i(k+1)\mathbf{n}_j^T(k+1)] = R_i \delta_{ij}$, where δ_{ij} is the Kronecker delta. Thus, the covariance corresponding to the measurement noise $\mathbf{n}(k+1) =$

¹In the remainder of the paper, the "hat" symbol, $\hat{\cdot}$, is used to denote the estimated value of a quantity, while the "tilde" symbol, $\tilde{\cdot}$, is used to signify the error between the actual value of a quantity and its estimate. The relationship between a variable, x , and its estimate, \hat{x} , is $\tilde{x} = x - \hat{x}$. Additionally, " \succ " and " \succeq " denote the matrix inequality in the positive definite and positive semidefinite sense, respectively.

$[\mathbf{n}_1^T(k+1), \dots, \mathbf{n}_M^T(k+1)]^T$ is $R = E[\mathbf{n}(k+1)\mathbf{n}^T(k+1)] = \text{diag}(R_i)$.

The measurement equation (4) is a nonlinear function of the state variable \mathbf{x}_T . The measurement-error equation, obtained by linearizing (4) is:

$$\begin{aligned} \tilde{\mathbf{z}}(k+1|k) &= \mathbf{z}(k+1) - \hat{\mathbf{z}}(k+1|k) \\ &\simeq H_{k+1} \tilde{\mathbf{x}}_T(k+1|k) + \mathbf{n}(k+1) \end{aligned} \quad (5)$$

where

$$\hat{\mathbf{z}}(k+1|k) = [\hat{z}_1^T(k+1|k), \dots, \hat{z}_M^T(k+1|k)]^T$$

$$\hat{z}_i(k+1|k) = [\hat{d}_i(k+1|k) \ \hat{\theta}_i(k+1|k)]^T$$

$$\hat{d}_i(k+1|k) = \sqrt{\widehat{\Delta x_{T_i}^2}(k+1|k) + \widehat{\Delta y_{T_i}^2}(k+1|k)}$$

$$\hat{\theta}_i(k+1|k) = \arctan\left(\frac{\widehat{\Delta y_{T_i}}(k+1|k)}{\widehat{\Delta x_{T_i}}(k+1|k)}\right) - \phi_i(k+1)$$

$$\widehat{\Delta x_{T_i}}(k+1|k) = \hat{x}_T(k+1|k) - x_{S_i}(k+1)$$

$$\widehat{\Delta y_{T_i}}(k+1|k) = \hat{y}_T(k+1|k) - y_{S_i}(k+1)$$

$$\tilde{\mathbf{x}}_T(k+1|k) = \mathbf{x}_T(k+1) - \hat{\mathbf{x}}_T(k+1|k)$$

Note that the measurement matrix in (5) has a block column structure, which is given by the following expression:

$$H_{k+1} = [H_{e,k+1} \ \mathbf{0}_{2M \times (2N-2)}] \quad (6)$$

where $2N$ is the dimension of the state vector and

$$H_{e,k+1} = [\mathbf{h}_1(k+1) \ \dots \ \mathbf{h}_M(k+1)] \quad (7)$$

$$\mathbf{h}_i(k+1) = [\mathbf{h}_{d_i}(k+1) \ \mathbf{h}_{\theta_i}(k+1)] \quad (8)$$

$$\mathbf{h}_{d_i}(k+1) = \frac{-1}{\sqrt{\mathbf{p}_i^T \mathbf{p}_i}} \mathbf{p}_i, \quad \mathbf{h}_{\theta_i}(k+1) = \frac{1}{\mathbf{p}_i^T \mathbf{p}_i} J \mathbf{p}_i \quad (9)$$

$$\mathbf{p}_i = \mathbf{p}_{S_i}(k+1) - \hat{\mathbf{p}}_T(k+1|k) \quad (10)$$

where $J = C(-\frac{\pi}{2})$ and $C(\cdot)$ is the 2×2 rotational matrix.

C. State and Covariance Update

Once the distance and bearing measurements, $\mathbf{z}(k+1)$, from all the sensors are available, the target's state estimate and its covariance are updated as:

$$\begin{aligned} \hat{\mathbf{x}}_T(k+1|k+1) &= \hat{\mathbf{x}}_T(k+1|k) + K_{k+1} \tilde{\mathbf{z}}(k+1|k) \\ P_{k+1|k+1} &= P_{k+1|k} - K_{k+1} S_{k+1} K_{k+1}^T \end{aligned} \quad (11)$$

where $K_{k+1} = P_{k+1|k} H_{k+1}^T S_{k+1}^{-1}$ is the Kalman gain, $S_{k+1} = H_{k+1} P_{k+1|k} H_{k+1}^T + R$ is the measurement residual covariance.

Our objective in this work is to determine the active sensing strategy that minimizes the uncertainty for the *position* estimate of the target. In order to account for the impact of the prior state estimates on the motion of the sensors, we first present the following lemma.

Lemma 1: The posterior (updated) covariance for the target's position estimate depends on (i) the prior (propagated) covariance sub-matrix of the target's *position* (i.e., it is independent of the uncertainty in the estimates of higher-order time derivatives of the position such as velocity, acceleration, etc., and hence it is independent of the target's motion model) and (ii) the measurement information matrix corresponding to the target's *position*, i.e.,

$$P_{k+1|k+1,11} = \left((P_{k+1|k,11})^{-1} + H_{e,k+1}^T R^{-1} H_{e,k+1} \right)^{-1} \quad (12)$$

where $P_{\ell|j,11}$ denotes the 2×2 upper diagonal sub-matrix of $P_{\ell|j}$ corresponding to the covariance in the position estimates.

Proof: The proof is shown in [13]. ■

The importance of this lemma is that the optimization algorithm presented in Section IV can be derived based on (12) for the position covariance update – instead of (11) for the entire state covariance update – regardless of the stochastic process model employed for describing the target's motion.

In the next section, we formulate the sensors' one-step-ahead *optimal motion strategy* as a constrained optimization problem, and discuss its properties.

D. Problem Statement and Reformulation

As evident from (7)-(10) and (12), after each update step the target's position covariance matrix will depend on all the next sensors' positions $\mathbf{p}_{S_i}(k+1) = [x_{S_i}(k+1) \ y_{S_i}(k+1)]^T$, $i = 1, \dots, M$. Assume that at time-step k , sensor- i is at location $\mathbf{p}_{S_i}(k) = [x_{S_i}(k) \ y_{S_i}(k)]^T$. At time-step $k+1$ its position $\mathbf{p}_{S_i}(k+1)$ is confined in a circular region centered at $\mathbf{p}_{S_i}(k)$, due to the maximum speed constraint, and outside a circular region centered at $\hat{\mathbf{p}}_T(k+1|k)$ to avoid collisions (cf. Fig. 1):

$$\|\mathbf{p}_{S_i}(k+1) - \mathbf{p}_{S_i}(k)\| \leq r_i = v_{i\max} \delta t \quad (13)$$

$$\|\mathbf{p}_{S_i}(k+1) - \hat{\mathbf{p}}_T(k+1|k)\| \geq \rho_i \quad (14)$$

Substituting \mathbf{p}_i [cf. (10)] in the above two equations, yields:

$$\|\mathbf{p}_i - [\mathbf{p}_{S_i}(k) - \hat{\mathbf{p}}_T(k+1|k)]\| \leq r_i \quad (15)$$

$$\|\mathbf{p}_i\| \geq \rho_i \quad (16)$$

where the feasible region of \mathbf{p}_i is inside a circle of radius r_i centered at $\mathbf{p}_{S_i}(k) - \hat{\mathbf{p}}_T(k+1|k)$, and outside a circle of radius ρ_i centered at the origin $[0, 0]^T$. Note that the estimate $\hat{\mathbf{p}}_T(k+1|k)$ [cf. (3)] is shared among all sensors, and can be treated as a constant at time-step $k+1$. Hence, once \mathbf{p}_i , $i = 1, \dots, M$, is determined, the location of sensor- i at time-step $k+1$, $\mathbf{p}_{S_i}(k+1)$, $i = 1, \dots, M$, can be obtained through (10).

The problem we address in this work is that of determining the sensors' *optimal motion strategy*, i.e., the set $\mathcal{C}(k+1) = \{\mathbf{p}_i, i = 1, \dots, M\}$, that minimizes the *trace* of the target's position estimate covariance matrix, under the constraints specified in (15)-(16). To proceed, we exploit the fact that R is a diagonal matrix, and substitute (7)-(9) in (12) to obtain the following optimization problem:

- OPTIMIZATION PROBLEM 1 (Π_1)

$$\begin{aligned} \min_{\mathbf{p}_1, \dots, \mathbf{p}_M} \quad & \text{tr} \left((P_{k+1|k,11})^{-1} + \sum_{i=1}^M \frac{1}{\sigma_{d_i}^2} \frac{\mathbf{p}_i \mathbf{p}_i^T}{\mathbf{p}_i^T \mathbf{p}_i} + \sum_{i=1}^M \frac{1}{\sigma_{\theta_i}^2} \frac{J \mathbf{p}_i \mathbf{p}_i^T J^T}{(\mathbf{p}_i^T \mathbf{p}_i)^2} \right)^{-1} \\ \text{s.t.} \quad & \|\mathbf{p}_i - [\mathbf{p}_{S_i}(k) - \hat{\mathbf{p}}_T(k+1|k)]\| \leq r_i, \\ & \|\mathbf{p}_i\| \geq \rho_i, \quad i = 1, \dots, M \end{aligned} \quad (17)$$

In what follows, we will consider, without loss of generality, the case $P_{k+1|k,11}$ being a diagonal matrix. If $P_{k+1|k,11}$

is non-diagonal, we can always apply a coordinate transformation (cf. Lemma 2), to transform it into a diagonal one.

Lemma 2: Assume $P_{k+1|k,11} \succ \mathbf{0}_{2 \times 2}$ is non-diagonal. The eigen-decomposition of $P_{k+1|k,11}^{-1} = C(\varphi_0) \Lambda C(-\varphi_0)$, and $\Lambda = \text{diag}(\lambda_1, \lambda_2)$, $\lambda_1 \geq \lambda_2 > 0$. Then,

$$\text{tr}(P_{k+1|k+1,11}) = \text{tr} \left(\Lambda + \sum_{i=1}^M \frac{1}{\sigma_{d_i}^2} \frac{\mathbf{s}_i \mathbf{s}_i^T}{\mathbf{s}_i^T \mathbf{s}_i} + \sum_{i=1}^M \frac{1}{\sigma_{\theta_i}^2} \frac{J \mathbf{s}_i \mathbf{s}_i^T J^T}{(\mathbf{s}_i^T \mathbf{s}_i)^2} \right)^{-1} \quad (18)$$

where $\mathbf{s}_i = C(-\varphi_0) \mathbf{p}_i$, $i = 1, \dots, M$.

Proof: Substituting $P_{k+1|k,11}^{-1} = C(\varphi_0) \Lambda C(-\varphi_0)$ and $\mathbf{p}_i = C(\varphi_0) \mathbf{s}_i$ in (17), employing the equality $C(-\varphi_0) J = J C(-\varphi_0)$ which holds since both are 2×2 rotational matrices, and noting that the trace operation is invariant to similarity transformations results in (18). ■

Note also that the similarity transformation does not change the norm of a vector; thus, constraint (15) is equivalent to $\|\mathbf{s}_i - \mathbf{c}_i\| \leq r_i$, with $\mathbf{c}_i = C(-\varphi_0) [\mathbf{p}_{S_i}(k) - \hat{\mathbf{p}}_T(k+1|k)]$, and constraint (16) is equivalent to $\|\mathbf{s}_i\| \geq \rho_i$. Therefore, from now on, we will mainly focus on the following equivalent optimization problem:

- OPTIMIZATION PROBLEM 2 (Π_2)

$$\min_{\mathbf{s}_1, \dots, \mathbf{s}_M} \quad \text{tr} \left(\Lambda + \sum_{i=1}^M \frac{1}{\sigma_{d_i}^2} \frac{\mathbf{s}_i \mathbf{s}_i^T}{\mathbf{s}_i^T \mathbf{s}_i} + \sum_{i=1}^M \frac{1}{\sigma_{\theta_i}^2} \frac{J \mathbf{s}_i \mathbf{s}_i^T J^T}{(\mathbf{s}_i^T \mathbf{s}_i)^2} \right)^{-1} \quad (19)$$

$$\text{s.t.} \quad \|\mathbf{s}_i - \mathbf{c}_i\|^2 \leq r_i^2, \quad (20)$$

$$\|\mathbf{s}_i\|^2 \geq \rho_i^2, \quad i = 1, \dots, M \quad (21)$$

Once the optimal solution $\{\mathbf{s}_i, i = 1, \dots, M\}$ is obtained, the best position of the i -th sensor at time-step $k+1$, $\mathbf{p}_{S_i}(k+1)$, can be calculated through $\mathbf{p}_i = C(\varphi_0) \mathbf{s}_i$ and (10).

Remark 1: The optimization problem Π_2 is a nonlinear programming problem since both the objective function [cf. (19)] and constraints [cf. (20)-(21)] are nonlinear functions with respect to the optimization variable $\mathbf{s} = [\mathbf{s}_1^T, \dots, \mathbf{s}_M^T]^T$. Moreover, Π_2 (and equivalently, Π_1) is not a convex programming since the feasible set defined by constraint (21) is not convex.

IV. PROBLEM SOLUTION

As mentioned in the previous section, the problem of *optimal trajectory generation* for multiple sensors with mobility constraints that track a moving target using distance and bearing measurements is *not convex* in general. Hence, finding the *global* optimal solution for the original optimization problem, or for its equivalent formulation (cf. $\Pi_1 \Leftrightarrow \Pi_2$), becomes challenging. Ideally, the optimal solution can be determined if one discretizes the feasible set of all sensors [cf. (20)-(21)] and performs an exhaustive search. This approach, however, has computational complexity *exponential* in the number of sensors, which is of limited practical use given realistic processing constraints.

In order to design algorithms that can operate in real time, appropriate relaxations of the original optimization problem become necessary. In what follows, we first present an analytic solution for the single-sensor case (cf. Section IV-A) and based on that we propose a *Gauss-Seidel relaxation*

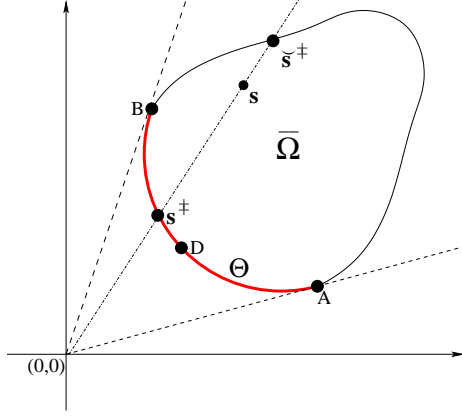


Fig. 2. Geometric illustration of Lemma 3. The global optimal solution resides only in a portion of the boundary of the feasible set $\bar{\Omega}$, which is denoted as Θ and depicted by the red-colored curve ADB .

(GSR) to solve the general problem of multiple sensors (cf. Section IV-B). The GSR algorithm has computational complexity *linear* in the number of sensors, which ensures real-time implementations even for a large number of sensors. Furthermore, as shown in Section V, GSR is able to achieve tracking accuracy indistinguishable of that of exhaustive search.

A. Single-sensor Target Tracking: Analytic-form Solution

For $M = 1$, the optimization problem described by (19)-(21) is simplified to:²

- OPTIMIZATION PROBLEM 3 (Π_3)

$$\min_{\mathbf{s}} f_0(\mathbf{s}) = \text{tr} \left(\Lambda + \frac{1}{\sigma_d^2} \mathbf{ss}^T + \frac{1}{\sigma_\theta^2} \frac{J\mathbf{ss}^T J^T}{(\mathbf{s}^T \mathbf{s})^2} \right)^{-1} \quad (22)$$

$$\text{s.t. } \|\mathbf{s} - \mathbf{c}\|^2 \leq r^2, \quad (23)$$

$$\|\mathbf{s}\|^2 \geq \rho^2 \quad (24)$$

In order to solve Π_3 , we proceed as follows: We first calculate *all critical points* (i.e., those points that satisfy the Karush-Kuhn-Tucker (KKT) necessary conditions) analytically and evaluate their objective values accordingly. Then, as global optimal solution for Π_3 we select the critical point whose objective value is the smallest.

To proceed, we first construct the Lagrange function:

$$L(\mathbf{s}, \mu, \nu) = f_0(\mathbf{s}) + \frac{\mu}{2} (\|\mathbf{s} - \mathbf{c}\|^2 - r^2) + \frac{\nu}{2} (\rho^2 - \|\mathbf{s}\|^2)$$

Based on the KKT necessary conditions [14, Ch. 3], the critical points \mathbf{s}^* , μ^* , and ν^* must satisfy all of the following relations:

$$\nabla f_0(\mathbf{s}^*) + \mu^* (\mathbf{s}^* - \mathbf{c}) - \nu^* \mathbf{s}^* = \mathbf{0}_{2 \times 1} \quad (25)$$

$$\mu^* \geq 0, \quad \mu^* (\|\mathbf{s}^* - \mathbf{c}\|^2 - r^2) = 0 \quad (26)$$

$$\nu^* \geq 0, \quad \nu^* (\rho^2 - \|\mathbf{s}^*\|^2) = 0 \quad (27)$$

The following lemma establishes the fact that the global optimal solution for Π_3 is always on the *boundary* of the feasible set, defined by (23)-(24), i.e., \mathbf{s}^* satisfies either $\|\mathbf{s}^* - \mathbf{c}\| = r$ or $\|\mathbf{s}^*\| = \rho$.

²To simplify notation, we drop the indices of \mathbf{s}_1 , σ_{d_1} , σ_{θ_1} , \mathbf{c}_1 , r_1 , ρ_1 .

Lemma 3: Assume $\bar{\Omega} = \Omega \cup \partial\Omega$ is a compact and connected set³ in 2D, and the origin $[0, 0]^T \notin \bar{\Omega}$. For any $\mathbf{s} \in \Omega$, the line segment connecting \mathbf{s} and the origin will inevitably intersect $\partial\Omega$ at one or multiple points, and $\mathbf{s}^\ddagger \in \partial\Omega$ denotes the one closest to $[0, 0]^T$ (cf. Fig. 2). Then $f_0(\mathbf{s}^\ddagger) \leq f_0(\mathbf{s})$.

Proof: Based on the construction of \mathbf{s}^\ddagger , we have: $\mathbf{s}^\ddagger = \epsilon \mathbf{s}$, with $\epsilon \in (0, 1)$, hence we conclude:

$$\begin{aligned} \frac{(\mathbf{s}^\ddagger)(\mathbf{s}^\ddagger)^T}{(\mathbf{s}^\ddagger)^T(\mathbf{s}^\ddagger)} &= \frac{\mathbf{ss}^T}{\mathbf{s}^T \mathbf{s}}, \quad \frac{J(\mathbf{s}^\ddagger)(\mathbf{s}^\ddagger)^T J^T}{((\mathbf{s}^\ddagger)^T(\mathbf{s}^\ddagger))^2} = \frac{1}{\epsilon^2} \frac{J\mathbf{ss}^T J^T}{(\mathbf{s}^T \mathbf{s})^2} \succeq \frac{J\mathbf{ss}^T J^T}{(\mathbf{s}^T \mathbf{s})^2} \Rightarrow \\ &\left(\Lambda + \frac{1}{\sigma_d^2} \frac{(\mathbf{s}^\ddagger)(\mathbf{s}^\ddagger)^T}{(\mathbf{s}^\ddagger)^T(\mathbf{s}^\ddagger)} + \frac{1}{\sigma_\theta^2} \frac{J(\mathbf{s}^\ddagger)(\mathbf{s}^\ddagger)^T J^T}{((\mathbf{s}^\ddagger)^T(\mathbf{s}^\ddagger))^2} \right)^{-1} \\ &\preceq \left(\Lambda + \frac{1}{\sigma_d^2} \frac{\mathbf{ss}^T}{\mathbf{s}^T \mathbf{s}} + \frac{1}{\sigma_\theta^2} \frac{J\mathbf{ss}^T J^T}{(\mathbf{s}^T \mathbf{s})^2} \right)^{-1} \end{aligned}$$

Therefore, $f_0(\mathbf{s}^\ddagger) \leq f_0(\mathbf{s})$. ■

Lemma 3 establishes the fact that the global optimal solution for Π_3 , when optimizing over the feasible set $\bar{\Omega}$ (cf. Fig. 2), is always attained on $\partial\Omega$. Moreover, by applying the same argument as before (cf. Fig. 2), it can be easily shown that $f_0(\mathbf{s}^\ddagger) \leq f_0(\mathbf{s}^\ddagger)$. Therefore, the global optimal solution \mathbf{s}^* resides only in the portion (the curve ADB) of $\partial\Omega$ facing the origin, denoted as Θ (cf. Fig. 2).

As shown in Figs. 3(a)–3(c), depending on the parameters \mathbf{c} , r , and ρ , there exist three cases we need to consider for the feasible set $\bar{\Omega}$ of Π_3 , described by the constraints (23)–(24). In what follows, we present the corresponding solutions satisfying the KKT conditions (25)–(27) for each of these three cases analytically. For clarity, we employ the following notation: $\mathbf{s}^* = [x \ y]^T$, and $\mathbf{c} = [c_1 \ c_2]^T$. Furthermore, we set $r = \min(v_{\max} \delta t, \|\mathbf{c}\|) \leq \|\mathbf{c}\|$.

1) *Case-I*, $\rho \leq \|\mathbf{c}\| - r$: As shown in Fig. 3(a), the only active constraint for Case-I is the maximum speed constraint [cf. (23)]. Based on Lemma 3 and setting $v = v_{\max}$, the optimal solution \mathbf{s}^* must reside on the red-colored arc ADB . Since the collision avoidance constraint (24) is inactive, its corresponding Lagrange multiplier is $\nu^* = 0$, and (25)–(27) are simplified to:

$$\nabla f_0(\mathbf{s}^*) + \mu^* (\mathbf{s}^* - \mathbf{c}) = \mathbf{0}_{2 \times 1} \quad (28)$$

$$\|\mathbf{s}^* - \mathbf{c}\|^2 - r^2 = 0 \quad (29)$$

Clearly, (29) is a 2nd order polynomial equation in the variables x and y , i.e.,

$$0 = f_2(x, y) = (x - c_1)^2 + (y - c_2)^2 - r^2 \quad (30)$$

Since we aim at transforming (28) into a polynomial equation only containing x and y , we eliminate μ^* by multiplying both sides of (28) with $(\mathbf{s}^* - \mathbf{c})^T C \left(\frac{\pi}{2}\right)$:

$$(\mathbf{s}^* - \mathbf{c})^T C \left(\frac{\pi}{2}\right) \nabla f_0(\mathbf{s}^*) = 0 \quad (31)$$

After rearranging terms in (31), we obtain the following 8th order polynomial equation in x and y :

$$0 = f_1(x, y) = \beta_3 xy \Delta^3 + (\alpha_8 x + \alpha_7 y + \beta_2) xy \Delta^2 \quad (32)$$

$$+ (\alpha_6 x^3 + \alpha_5 x^2 y + \alpha_4 xy^2 + \alpha_3 y^3 + \beta_1 xy) \Delta + (\alpha_2 x + \alpha_1 y) xy$$

where $\Delta := x^2 + y^2$, and the parameters α_i , $i = 1, \dots, 8$,

³ Ω stands for the open set consisting of all interior points of $\bar{\Omega}$, while $\partial\Omega$ and $\bar{\Omega}$ represent its boundary and closure, respectively.

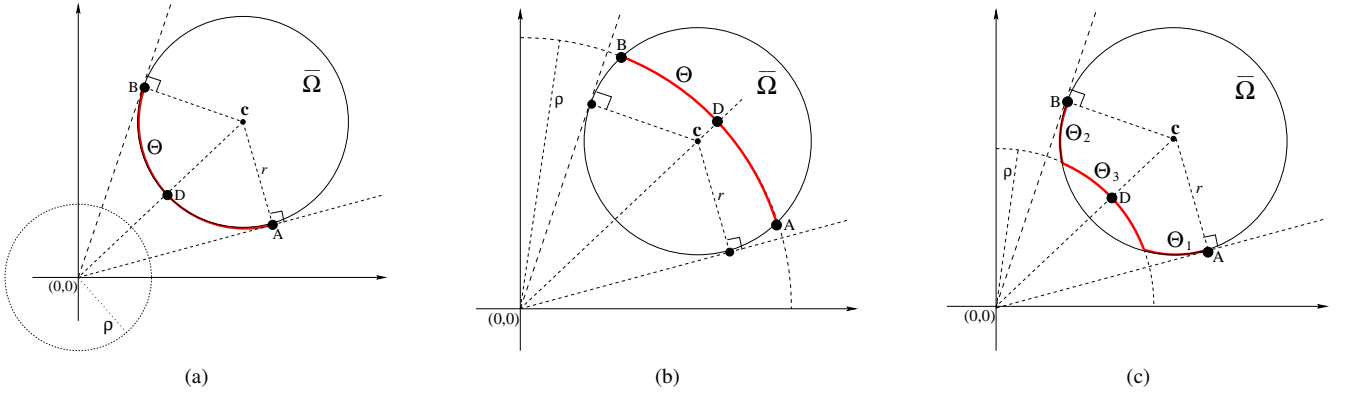


Fig. 3. Feasible set $\bar{\Omega}$ of s . (a) Case-I: $\rho \leq \|c\| - r$. (b) Case-II: $\rho \geq \sqrt{\|c\|^2 - r^2}$. (c) Case-III: $\|c\| - r < \rho < \sqrt{\|c\|^2 - r^2}$. In all three cases, the global optimal solution resides in a subset of the boundary of $\bar{\Omega}$, which is denoted as Θ and depicted by the red-colored curve ADB .

and β_i , $i = 1, 2, 3$, are known coefficients expressed in terms of $\lambda_1, \lambda_2, c_1, c_2, \sigma_d^2, \sigma_\theta^2$, and r . Due to space limitations, the interested reader can refer to [13] for more details.

In order to obtain all the critical points of Π_3 in Case-I, we need to solve the two polynomial equations $f_2(x, y) = 0$ and $f_1(x, y) = 0$ analytically [cf. (30) and (32)]. By employing the Sylvester resultant [15, Ch. 3], we are able to eliminate variable y from (30) and (32), and obtain the following 10th order univariate polynomial in variable x :

$$0 = f_3(x) = \sum_{j=0}^{10} \gamma_j x^j \quad (33)$$

where γ_j , $j = 0, \dots, 10$, are known coefficients expressed in terms of $\lambda_1, \lambda_2, c_1, c_2, \sigma_d^2, \sigma_\theta^2$, and r [13].

The roots of f_3 are the eigenvalues of the corresponding 10×10 companion matrix [1], [13]. Although there are 10 solutions for x , we only need to consider the real eigenvalues of the companion matrix. Once x is determined, y is computed from (30), and the critical point $[x, y]^T$ is added into the set $\bar{\Xi}_1$, which has at most 20 elements.

The final step is to evaluate the objective function $f_0(s)$ [cf. (22)] at all the critical points in $\bar{\Xi}_1$ and select the one with the smallest objective value as the global optimal solution for Π_3 .

2) *Case-II*, $\rho \geq \sqrt{\|c\|^2 - r^2}$: As shown in Fig. 3(b) and based on Lemma 3, the only active constraint for Case-II is the collision avoidance constraint [cf. (24)]. Since the maximum speed constraint (23) is inactive, its corresponding Lagrange multiplier $\mu^* = 0$, and (25)-(27) are simplified to:

$$\nabla f_0(s^*) - \nu^* s^* = \mathbf{0}_{2 \times 1} \quad (34)$$

$$\|s^*\|^2 - \rho^2 = 0 \quad (35)$$

Clearly, (35) is a 2nd order bivariate polynomial equation, i.e.,

$$0 = f_5(x, y) = x^2 + y^2 - \rho^2 \quad (36)$$

Applying the same technique as in Case-I to eliminate ν^* in (34), yields:

$$0 = f_4(x, y) = xy \quad (37)$$

It is easy to verify that the four real solutions satisfying (36) and (37) are $\{[\pm\rho \ 0]^T, [0 \ \pm\rho]^T\}$. However, not all these critical points necessarily belong to the feasible

region $\bar{\Omega}$, or equivalently, reside in the arc ADB , which is defined by (35) and inside the disk characterized by (23) [cf. Fig 3(b)]. Hence, the set $\bar{\Xi}_2$ containing all the *feasible* critical points can possibly have zero, and up to four elements. In particular, for the plot shown in Fig. 3(b), $\bar{\Xi}_2 = \emptyset$. Note, however, that since the curve ADB is an arc of the circle defined by (35), it is also necessary to consider the objective value attained at the two boundary points A and B [cf. Fig. 3(b)]. Thus, the set $\bar{\Xi}_2$ is augmented into $\bar{\Xi}_2 = \bar{\Xi}_2 \cup \{A, B\}$, which contains at least two, and up to six elements. The global optimal solution for Π_3 in Case-II is selected as $s^* \in \bar{\Xi}_2$ the one with the smallest objective value $f_0(s^*)$.

3) *Case-III*, $\rho \in (\|c\| - r, \sqrt{\|c\|^2 - r^2})$: As shown in Fig. 3(c) and based on Lemma 3, the optimal solution $s^* \in \bar{\Omega}$ must reside in the red-colored curve ADB , which is composed of three segments, i.e., $\Theta = \Theta_1 \cup \Theta_2 \cup \Theta_3$. Here, Θ_1 and Θ_2 are due to the maximum speed constraint (23), and Θ_3 is because of the collision avoidance constraint (24).

To obtain the critical points in Case-III, we proceed as follows: We first ignore the collision avoidance constraint (24) and calculate the set $\bar{\Xi}_1$ of all critical points of Π_3 under the maximum speed constraint (23), following the process outlined in Case-I. Then, we apply the method outlined in Case-II to compute the optimal solution s^\dagger of Π_3 , while confining the feasible set to Θ_3 only. Since Θ_1 and Θ_2 are two arcs of the circle defined by (29), it is also necessary to consider the objective value attained at the two boundary points A and B [cf. Fig. 3(c)]. Based on the above strategy, the set of all critical points in Case-III, denoted as $\bar{\Xi}_3$, satisfies $\bar{\Xi}_3 \subseteq \bar{\Xi}$, where $\bar{\Xi} = \bar{\Xi}_1 \cup \{s^\dagger, A, B\}$, which is a finite set with cardinality at most 23.

The final step is to evaluate the objective function $f_0(s)$ at all the critical points in $\bar{\Xi}_3$, and select the s^* with the smallest objective value $f_0(s^*)$ as the global optimal solution for Π_3 .

B. Multiple-sensor Target Tracking: Gauss-Seidel Relaxation

Motivated by the simplicity of the analytic-form solution for the case of one sensor (cf. Section IV-A), a straightforward approach to finding a minimum of the optimization problem Π_2 is to iteratively minimize its objective function

[cf. (19)] for each optimization variable separately, i.e., [16, Ch. 3]:

- OPTIMIZATION PROBLEM 4 (Π_4)

$$\begin{aligned} \min_{\mathbf{s}_i^{(\ell+1)}} \operatorname{tr} & \left(\left(P_i^{(\ell+1)} \right)^{-1} + \frac{1}{\sigma_{d_i}^2} \frac{\left(\mathbf{s}_i^{(\ell+1)} \right) \left(\mathbf{s}_i^{(\ell+1)} \right)^T}{\left(\mathbf{s}_i^{(\ell+1)} \right)^T \left(\mathbf{s}_i^{(\ell+1)} \right)} \right. \\ & \left. + \frac{1}{\sigma_{\theta_i}^2} \frac{J \left(\mathbf{s}_i^{(\ell+1)} \right) \left(\mathbf{s}_i^{(\ell+1)} \right)^T J^T}{\left(\left(\mathbf{s}_i^{(\ell+1)} \right)^T \left(\mathbf{s}_i^{(\ell+1)} \right) \right)^2} \right)^{-1} \quad (38) \\ \text{s.t. } & \left\| \mathbf{s}_i^{(\ell+1)} - \mathbf{c}_i \right\| \leq r_i \quad \text{and} \quad \left\| \mathbf{s}_i^{(\ell+1)} \right\| \geq \rho_i \end{aligned}$$

where $\mathbf{s}_i^{(\ell+1)}$ is the sought new optimal value of \mathbf{s}_i at iteration $\ell + 1$, and $P_i^{(\ell+1)}$ is defined as:

$$\begin{aligned} \left(P_i^{(\ell+1)} \right)^{-1} &= \Lambda + \\ & \sum_{j=i+1}^M \left(\frac{1}{\sigma_{d_j}^2} \frac{\left(\mathbf{s}_j^{(\ell)} \right) \left(\mathbf{s}_j^{(\ell)} \right)^T}{\left(\mathbf{s}_j^{(\ell)} \right)^T \left(\mathbf{s}_j^{(\ell)} \right)} + \frac{1}{\sigma_{\theta_j}^2} \frac{J \left(\mathbf{s}_j^{(\ell)} \right) \left(\mathbf{s}_j^{(\ell)} \right)^T J^T}{\left(\left(\mathbf{s}_j^{(\ell)} \right)^T \left(\mathbf{s}_j^{(\ell)} \right) \right)^2} \right) + \\ & \sum_{j=1}^{i-1} \left(\frac{1}{\sigma_{d_j}^2} \frac{\left(\mathbf{s}_j^{(\ell+1)} \right) \left(\mathbf{s}_j^{(\ell+1)} \right)^T}{\left(\mathbf{s}_j^{(\ell+1)} \right)^T \left(\mathbf{s}_j^{(\ell+1)} \right)} + \frac{1}{\sigma_{\theta_j}^2} \frac{J \left(\mathbf{s}_j^{(\ell+1)} \right) \left(\mathbf{s}_j^{(\ell+1)} \right)^T J^T}{\left(\left(\mathbf{s}_j^{(\ell+1)} \right)^T \left(\mathbf{s}_j^{(\ell+1)} \right) \right)^2} \right) \end{aligned}$$

where $\mathbf{s}_j^{(\ell+1)}$, $j = 1, \dots, i - 1$, and $\mathbf{s}_j^{(\ell)}$, $j = i + 1, \dots, M$, are the remaining optimization variables, considered fixed during this step, computed sequentially during the previous iterations.

Note that the matrix $P_i^{(\ell+1)}$ is positive definite, and in general, non-diagonal. However, based on Lemma 2, through a similarity transformation, the optimization method employed in the single-sensor case (cf. Section IV-A) can be readily applied to solve Π_4 . Moreover, the optimization process in the Gauss-Seidel relaxation (GSR) algorithm is carried out only for one variable (i.e., \mathbf{s}_i) at every step. Thus, the GSR process has computational complexity only *linear* in the number of sensors. Furthermore, it is easily implemented, has low memory requirements and, as demonstrated in Section V, it achieves the same level of positioning accuracy as the exhaustive search approach.

V. SIMULATION RESULTS

In order to evaluate the presented *constrained* optimal motion strategy, Gauss-Seidel Relaxation (GSR), we have conducted extensive simulation experiments and compared the performance of GSR to the following methods:⁴

- *Grid-Based Exhaustive Search* (GBES). In this case, we discretize the feasible set of all sensors and perform an exhaustive search over all possible combinations of these to find the one that minimizes the trace of the covariance matrix for the target's position estimates. Ideally, the GBES should return the global optimal solution and it could be used as a benchmark for evaluating the GSR, if the grid size

⁴Due to space limitations we only describe here the results for the case of a team with 3 heterogeneous sensors. Further studies are presented in [13].

is sufficiently small. However, this is difficult to guarantee in practice since its computational complexity and memory requirements are exponential in the number of sensors. Hence implementing the GBES becomes prohibitive when the number of sensors, M , increases and/or when the size of the grid cells decreases.

- *Random Motion* (RM). This is a modification of an intuitive strategy that would require the sensors to move towards the target. In this case, however, and in order to ensure that the sensors do not converge to the same point, we require that at every time step sensor- i selects its heading direction with uniform probability towards points within the curve ADB shown in Figs. 3(a)–3(c).

1) *Simulation Setup*: For the purposes of this simulation, we adopt a zero-acceleration target motion model

$$\dot{\mathbf{x}}_T(t) = F \mathbf{x}_T(t) + G \mathbf{w}(t) \quad (39)$$

where

$$F = \begin{bmatrix} 0 & 0 & 1 & 0 \\ 0 & 0 & 0 & 1 \\ 0 & 0 & 0 & 0 \\ 0 & 0 & 0 & 0 \end{bmatrix}, \quad G = \begin{bmatrix} 0 & 0 \\ 0 & 0 \\ 1 & 0 \\ 0 & 1 \end{bmatrix}, \quad \mathbf{x}_T(t) = \begin{bmatrix} x_T(t) \\ y_T(t) \\ \dot{x}_T(t) \\ \dot{y}_T(t) \end{bmatrix},$$

and $\mathbf{w}(t) = [w_x(t) \ w_y(t)]^T$ is a zero-mean white Gaussian noise vector with covariance $E[\mathbf{w}(t)\mathbf{w}^T(\tau)] = qI_2\delta(t-\tau)$, $q = 10$, and $\delta(t-\tau)$ is the Dirac delta. In our implementation, we discretize the continuous-time system model [cf. (39)] with time step $\delta t = 0.1$ sec.

The initial true state of the target is $\mathbf{x}_T(0) = [0, 0, -8, 6]^T$. The initial estimate for the target's state is $\hat{\mathbf{x}}_T(0) = [2, -2, 0, 0]^T$. This can be obtained by processing the first measurements from the sensors at time-step 0. At the beginning of the experiment, the sensors are randomly distributed within a circle of radius 5 m, which is at a distance of about 20 m from the target's initial position. The maximum speed for each sensor is set to 10 m/s, i.e., the largest distance that a sensor can travel during any time step is 1 m. The minimum distance between the target and sensors is set to $\rho = 2$ m. The duration of the simulations is 5 sec (i.e., 50 time steps). At every time step, we employ the methods described (i.e., GBES, GSR, and RM) to calculate the next sensing location of each sensor. Throughout the simulations, we set the GBES cell size to $\pi/200$; i.e., we discretize the curve ADB [cf. Figs. 3(a)–3(c)] in segments of length $\pi/200$ m.

Finally, the measurement noise covariance matrix for the three sensors considered is set to $R_i = \operatorname{diag}(\sigma_{d_i}^2, \sigma_{\theta_i}^2)$, with $\sigma_{d_1}^2 = 2 \text{ m}^2$, $\sigma_{d_2}^2 = \sigma_{d_3}^2 = 4 \text{ m}^2$, $\sigma_{\theta_1}^2 = 0.25 \text{ rad}^2$, and $\sigma_{\theta_2}^2 = \sigma_{\theta_3}^2 = 0.5 \text{ rad}^2$.

2) *Target Tracking with 3 Sensors (Heterogeneous team)*: Figs 4(a)–4(c) depict the actual and estimated trajectories of the target, along with the trajectories of the three sensors, when employing as motion strategy GBES, GSR, and RM, respectively. As evident, the accuracy of the target's position estimates for GSR is significantly better than that of RM and almost identical to that of GBES. Furthermore, the EKF estimates from the GSR and GBES are consistent.

Interestingly, in this case the heterogeneous sensor team splits into two groups. Sensor-1 (the most accurate one with

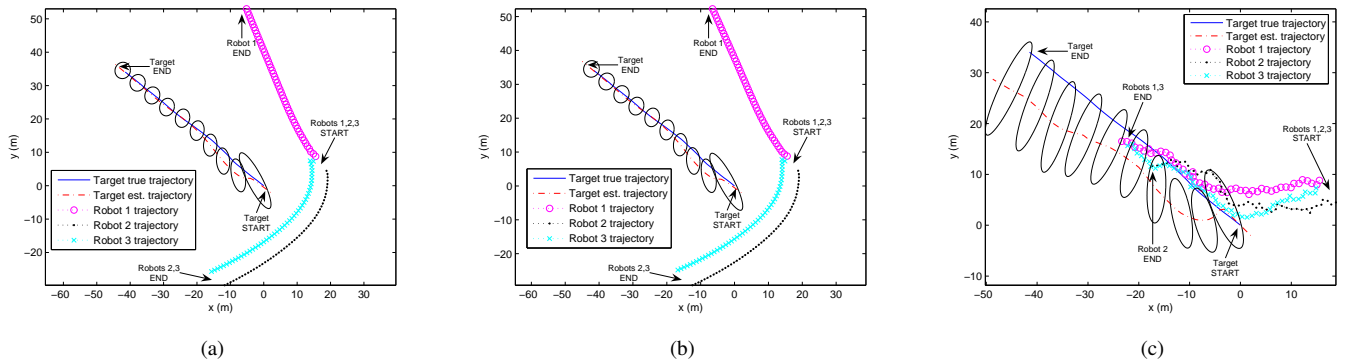


Fig. 4. [3-Sensors case] Trajectories of the three sensors, and the actual and estimated trajectories of the target, when employing as motion strategy (a) GBES, (b) GSR, and (c) RM. The ellipses denote the 3σ bounds for the target's position uncertainty at the corresponding time steps.

measurement noise variances $\sigma_{d_1}^2 = 2 \text{ m}^2$, $\sigma_{\theta_1}^2 = 0.25 \text{ rad}^2$) follows the target from the right, while sensors 2 and 3 form a separate cluster approaching the target from the left while moving very close to each other. The reason for this is the following: As sensors 2 and 3 measure their distance and bearing to the target from approximately the same location at every time step, their four independent measurements become equivalent, in terms of accuracy, to two with variances

$$\frac{1}{\sigma_{d_{2,3}}^2} \simeq \frac{1}{\sigma_{d_2}^2} + \frac{1}{\sigma_{d_3}^2} = \frac{1}{2}, \text{ or } \sigma_{d_{2,3}}^2 \simeq 2$$

$$\frac{1}{\sigma_{\theta_{2,3}}^2} \simeq \frac{1}{\sigma_{\theta_2}^2} + \frac{1}{\sigma_{\theta_3}^2} = 4, \text{ or } \sigma_{\theta_{2,3}}^2 \simeq 0.25$$

Hence, this problem becomes equivalent to that of 2 sensors with equal distance and bearing noise variances [13], with the difference that in this case the "second" sensor is realized by requiring sensors 2 and 3 to move close to each other.

VI. CONCLUSIONS

In this paper, we address the problem of determining *optimal trajectories* for a team of heterogeneous sensors (robots) that track a moving target using *distance and bearing* measurements. The optimality criterion used is the minimization of the trace of the target's position covariance matrix. In our formulation, we have accounted for the existence of *prior information* and considered motion constraints on the robots (maximum speed and minimum distance to the target). We have shown that this non-linear constrained optimization problem is non-convex, in general, and have derived the optimal solution for the single-robot case in *analytical form*. Moreover, and in order to provide real-time solutions, we have introduced an iterative algorithm, Gauss-Seidel relaxation (GSR), for generating optimal trajectories for a team of robots whose computational and memory requirements are significantly lower compared to those of a grid-based exhaustive search (GBES) method (linear vs. exponential in the number of robots). Simulation studies demonstrate that the GSR achieves the same level of tracking accuracy as GBES, and significantly better when compared to the case when the robots move randomly towards the target.

In our future work, we plan to extend our current approach and address the cases when the robots' poses are uncertain

and when multiple targets are present. Finally, we intend to consider additional constraints both on the visibility and the motion of the robots due to obstacles in their surroundings.

REFERENCES

- [1] A. Edelman and H. Murakami, "Polynomial roots from companion matrix eigenvalues," *Mathematics of Computation*, vol. 64, no. 210, pp. 763–776, Apr. 1995.
- [2] K. C. Chang, R. K. Saha, and Y. Bar-Shalom, "On optimal track-to-track fusion," *IEEE Trans. on Aerospace and Electronic Systems*, vol. 33, no. 4, pp. 1271–1276, Oct. 1997.
- [3] E. J. Msechu, S. I. Roumeliotis, A. Ribeiro, and G. B. Giannakis, "Distributed quantized Kalman filtering with scalable communication cost," *IEEE Trans. on Signal Processing*, vol. 56, no. 8, pp. 3727–3741, Aug. 2008.
- [4] E. W. Frew, "Trajectory design for target motion estimation using monocular vision," Ph.D. dissertation, Stanford University, Stanford, CA, Aug. 2003.
- [5] J. M. Passerieux and D. Van Cappel, "Optimal observer maneuver for bearings-only tracking," *IEEE Trans. on Aerospace and Electronic Systems*, vol. 34, no. 3, pp. 777–788, Jul. 1998.
- [6] J. R. Spletzer and C. J. Taylor, "Dynamic sensor planning and control for optimally tracking targets," *The International Journal of Robotics Research*, vol. 22, no. 1, pp. 7–20, Jan. 2003.
- [7] S. Martínez and F. Bullo, "Optimal sensor placement and motion coordination for target tracking," *Automatica*, vol. 42, no. 4, pp. 661–668, Apr. 2006.
- [8] P. Yang, R. A. Freeman, and K. M. Lynch, "Distributed cooperative active sensing using consensus filters," in *Proc. of the IEEE Int. Conf. on Robotics and Automation*, Rome, Italy, Apr. 10-14 2007, pp. 405–410.
- [9] K. Zhou and S. I. Roumeliotis, "Optimal motion strategies for range-only constrained multisensor target tracking," *IEEE Trans. on Robotics*, vol. 24, no. 5, pp. 1168–1185, Oct. 2008.
- [10] A. W. Stroupe and T. Balch, "Value-based action selection for observation with robot teams using probabilistic techniques," *Robotics and Autonomous Systems*, vol. 50, no. 2-3, pp. 85–97, Feb. 2005.
- [11] T. H. Chung, J. W. Burdick, and R. M. Murray, "A decentralized motion coordination strategy for dynamic target tracking," in *Proc. of the IEEE Int. Conf. on Robotics and Automation*, Orlando, FL, May 15-19 2006, pp. 2416–2422.
- [12] Y. Bar-Shalom, X. R. Li, and T. Kirubarajan, *Estimation with Applications to Tracking and Navigation*. New York, NY: Wiley-Interscience, John Wiley & Sons Inc., 2001.
- [13] K. Zhou and S. I. Roumeliotis, "Optimal motion strategies for range and bearing constrained multisensor target tracking," MARS Lab, Dept. of Computer Science and Engineering, University of Minnesota, Tech. Rep., Feb. 2009, <http://mars.cs.umn.edu/tr/reports/Ke09-2.pdf>.
- [14] D. P. Bertsekas, *Nonlinear Programming*, 2nd ed. Belmont, MA: Athena Scientific, 1999.
- [15] D. A. Cox, J. B. Little, and D. O'Shea, *Ideals, Varieties, and Algorithms: An Introduction to Computational Algebraic Geometry and Commutative Algebra*, 3rd ed. New York, NY: Springer, 2007.
- [16] D. P. Bertsekas and J. N. Tsitsiklis, *Parallel and Distributed Computation: Numerical Methods*. Belmont, MA: Athena Scientific, 1997.